Supporting Information for

Controllable Synthesis of Up-Conversion Luminescent Gd/Tm-MOFs promising for pH-Responsive Delivery and Dual-Modal Imaging

Table of Contents:

Table S1. Reports on MOFs with UCL.

Metal ions	Ligand	Excitation wavelength (nm)	Lifetime (μs)	Quantum Yield	Application	Ref
Tb^{3+}	N-[2-(bis{2-[(2-methoxybenzoyl)amino] ethyl}amino)ethyl] -2-methoxybenzamide	845	—	—	—	1
Y^{3+}, Yb^{3+}, Er^{3+}	1,4-benzenedicarboxylate	980	—	—	—	2
Y^{3+}, Er^{3+}	1,3,5-benzenetricarboxylic acid	980	113.89	—	Ibuprofen delivery	3
Y^{3+}, Yb^{3+}, Er^{3+}	Oxalate anion and 4,4'-oxybis(benzoic acid)	980	—	—	—	4
Y^{3+}, Yb^{3+}, Er^{3+}	2,3-pyrazinedicarboxylic acid	975	—	—	—	5
Y^{3+}, Yb^{3+}, Er^{3+}	pyrazine-2,3-carboxylic acid	974	—	—	—	6
Nd^{3+}/Gd^{3+}/Pr^{3+}/Ce^{3+}/Sm^{3+}	anthracene dicarboxylate & dimethylacetamide	800	—	—	—	7
Er^{3+}/Ho^{3+}, Na^{+}	pyrazine-2,3,5-tricarboxylate	980	—	—	—	8
Er^{3+}	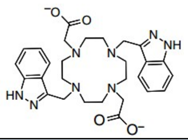	980	—	—	—	9
Gd^{3+}, Tm^{3+}	1,3,5-benzenetricarboxylic acid	980	τ=379±2	0.76 %	Drug delivery, UCL/MRI dual-mode imaging	**This work**

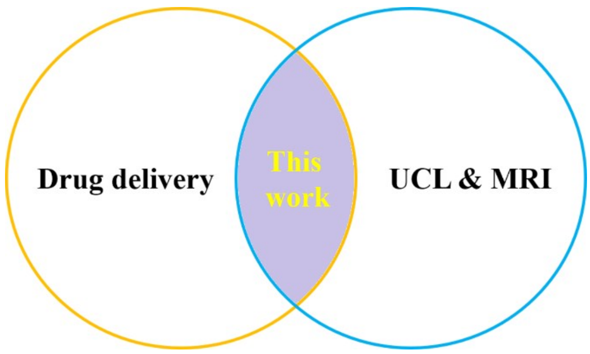

Figure S1. Pie chart of reports on MOFs with up-conversion luminescence.

References:

1. Wong, K. L.; Kwok, W. M.; Wong, W. T.; Phillips, D. L.; Cheah, K. W. Green and Red Three-Photon Upconversion from Polymeric Lanthanide(III) Complexes. *Angew. Chem.* **2004**, *116,* 4759–4762.
2. Weng, D. F.; Zheng, X. J.; Jin, L. P. Assembly and Upconversion Properties of Lanthanide Coordination Polymers Based on Hexanuclear Building Blocks with (μ_3-OH) Bridges. *Eur. J. Inorg. Chem.* **2006**, 4184–4190.
3. Zhang, X. D.; Li, B.; Ma, H. P.; Zhang, L. M.; Zhao, H. F. Metal−Organic Frameworks Modulated by Doping Er^{3+} for Up-Conversion Luminescence. *ACS Appl. Mat. Interfaces.* **2017**, *9,* 2594–2605.
4. Sun, C. Y.; Zheng, X. J.; Chen, X. B.; Li, L. C.; Jin, L. P. Assembly and Upconversion Luminescence of Lanthanide–Organic Frameworks with Mixed Acid Ligands. *Inorg. Chim. Acta* **2009**, *362,* 325–330.
5. Weng, D.F.; Zheng, X.J.; Chen, X.B.; Li, L.C.; Jin, L.P. Synthesis, Upconversion Luminescence and Magnetic Properties of New Lanthanide-Organic Frameworks with $(4^3)_2(4^6, 6^6, 8^3)$ Topology. *Eur. J. Inorg. Chem.* **2007**, *21,* 3410–3415.
6. Giedraityte, Z. Tuomisto, M. Lastusaari, M. Karppinen, M. Three- and Two-Photon NIR-to-Vis (Yb,Er) Upconversion from ALD/MLD-Fabricated Molecular Hybrid Thin Films. *ACS Appl. Mater. Interfaces* **2018**, *10 (10)*, 8845–8852.
7. Quah, H. S.; Ng, L. T.; Donnadieu, B.; Tan, G. K.; Vittal, J. J. Molecular Scissoring: Facile 3D to 2D Conversion of Lanthanide Metal Organic Frameworks Via Solvent Exfoliation. *Inorg. Chem.* **2016**, *55*, 10851–10854.
8. Zheng, X. J.; Ablet, A.; Ng, C.; Wong, W. T. Intensive Upconversion Luminescence of Na-Codoped Rare-Earth Oxides with a Novel RE–Na Heterometallic Complex as Precursor. *Inorg. Chem.* **2014**, *53*, 6788–6793.
9. Nonat, A.; Chan, C. F.; Liu, T.; Platas-Iglesias, C.; Liu, Z.; Wong, W. T.; Wong, W. K.; Wong, K. L.; Charbonnière, L. J. Room Temperature Molecular Up Conversion in Solution. *Nat. Commun.* **2016**, *7*, 11978.

Table S2. Homogenous materials integrating with UCL/MRI.

Structure of materials	**Application**	**Ref**
Gd_2O_3:Yb^{3+}/Ln^{3+} UCNs	UCL, MRI	1–3
Gd_2O_3:Yb^{3+}/Er^{3+}	UCL, MRI, CT	4
Gd_2O_3 hollow spheres	Drug delivery, UCL, MRI	5
$GdPO_4$:Yb,Er	UCL, MRI	6
$NaY_{0.2}Gd_{0.6}Yb_{0.18}Er_{0.02}F_4$	UCL, MRI, PET	7
$BaGdF_5$:Yb/Er	UCL, MRI, CT	8
$NaGdF_4$: Yb^{3+}, Ln^{3+}	UCL, MRI	9–13
$NaLuF_4$:Yb^{3+}, Tm^{3+}, Gd^{3+}	UCL, MRI	14
Gd^{3+}-$Zn_{2.94}Ga_{1.96}Ge_2O_{10}$:$Cr^{3+}$,$Pr^{3+}$	UCL, MRI	15
Dy_2O_3:Tb^{3+}	UCL, MRI	16
$Gd_2Mo_3O_9$: Er^{3+}/Yb^{3+}	UCL, MRI	17
$NaYbF_4$: Tm^{3+}/Gd^{3+}	UCL, MRI	18
$BaYbF_5$:Gd/Er	UCL, MRI, CT	19
Ba_2GdF_7:Yb^{3+}, Er^{3+}	UCL, MRI	20
$NaYF_4$: Yb^{3+}, Er^{3+}/Gd^{3+}	UCL, MRI, CT	21
β-$Ca_3(PO_4)_2$: Gd^{3+}, Dy^{3+}, Yb^{3+}	UCL, MRI, CT	22
Mn^{2+} doped $NaLuF_4$:Yb/Er	UCL, MRI, CT	23
(Gd^{3+}, Tm^{3+})(BTC)•(H_2O)•DMF	Drug delivery, UCL, MRI	**This work**

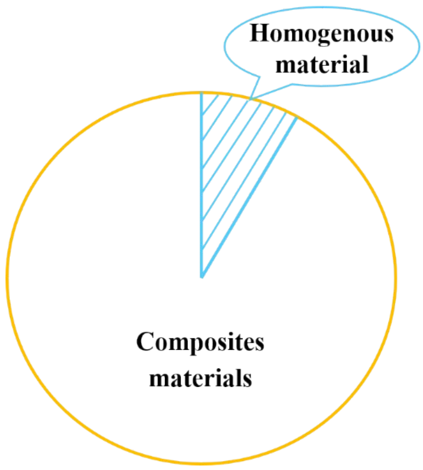

Figure S2. Pie chart of reports on multifunctional materials integrating with UCL/MRI.

References:

1. Liu, J.; Huang, L.; Tian, X. M.; Chen, X. M.; Shao, Y. G.; Xie, F. K.; Chen, D. H.; Li, L. Magnetic and Fluorescent Gd_2O_3:Yb^{3+}/Ln^{3+} Nanoparticles for Simultaneous Upconversion Luminescence/MR Dual Modal Imaging and NIR-Induced Photodynamic Therapy. *Int. J. Nanomed.* **2017**, *12*, 1–14.
2. Zhou, L. J.; Gu, Z. J.; Liu, X. X.; Yin, W. Y.; Tian, G.; Yan, L.; Jin, S.; Ren, W. L.; G. Xing, M.; Li, W.; Chang, X. L.; Hu, Z. B.; Zhao, Y. L. Size-Tunable Synthesis of Lanthanide-Doped Gd_2O_3 Nanoparticles and Their Applications for Optical and Magnetic Resonance Imaging. *J. Mater. Chem.* **2012**, *22*, 966–974.
3. Das, G. K.; Heng, B. C.; Ng, S. C.; White, T.; Loo, J. S. C.; D'Silva, L.; Padmanabhan, P.; Bhakoo, K. K.; Selvan, S. T.; Tan, T. T. Y. Gadolinium Oxide Ultranarrow Nanorods as Multimodal Contrast Agents for Optical and Magnetic Resonance Imaging. *Langmuir*. **2010**, *26*, 8959–8965.
4. Liu, Z.; Pu, F.; Huang, S.; Yuan, Q.; Ren, J.; Qu, X. Long-Circulating Gd_2O_3:Yb^{3+}, Er^{3+} Up-Conversion Nanoprobes as High-Performance Contrast Agents for Multi-Modality Imaging. *Biomaterials* **2013**, *34*, 1712–1721.
5. Tian, G.; Gu, Z. J.; Liu, X. X.; Zhou, L. J.; Yin, W. Y.; Yan, L.; Jin, S.; Ren, W. L.; Xing, G. M.; Li, S. J.; Zhao, Y. L. Facile Fabrication of Rare-Earth-Doped Gd_2O_3 Hollow Spheres with Upconversion Luminescence, Magnetic Resonance, and Drug Delivery Properties. *J. Phys. Chem. C* **2011**, *115*, 23790–23796.
6. Ren, W. L.; Tian, G.; Zhou, L. J.; Yin, W. Y.; Yan, L.; Jin, S.; Zu, Y.; Li, S. J.; Gu, Z. J.; Zhao, Y. L. Lanthanide Ion-Doped $GdPO_4$ Nanorods with Dual-Modal Bio-Optical and Magnetic Resonance Imaging Properties. *Nanoscale* **2012**, *4*, 3754–3760.
7. Zhou, J.; Yu, M. X.; Sun, Y.; Zhang, X. Z.; Zhu, X. J.; Wu, Z. H.; Wu, D. M.; Li, F. Y. Fluorine-18-Labeled Gd^{3+}/Yb^{3+}/Er^{3+} Co-Doped $NaYF_4$ Nanophosphors for Multimodality

PET/MR/UCL Imaging. *Biomaterials* **2011**, *32*, 1148–1156.

8. Zeng, S.; Tsang, M. K.; Chan, C. F.; Wong, K. L.; Hao, J. PEG Modified $BaGdF_5$:Yb/Er Nanoprobes for Multi-Modal Upconversion Fluorescent, in *Vivo* X-Ray Computed Tomography and Biomagnetic Imaging. *Biomaterials* **2012**, *33*, 9232–9238.
9. Zhou, J.; Sun, Y.; Du, X.; Xiong, L.; Hu, H.; Li, F. Y. Dual-Modality in *Vivo* Imaging Using Rare-Earth Nanocrystals with Near-Infrared to Near-Infrared (NIR-to-NIR) Upconversion Luminescence and Magnetic Resonance Properties. *Biomaterials* **2010**, 31, 3287–3295.
10. Ryu, J.; Park, H. Y.; Kim, K.; Kim, H.; Yoo, J. H.; Kang, M.; Im, K.; Grailhe, R.; Song, R. Facile Synthesis of Ultrasmall and Hexagonal $NaGdF_4$: Yb^{3+}, Er^{3+} Nanoparticles with Magnetic and Upconversion Imaging Properties. *J. Phys. Chem. C* **2010**, *114*, 21077–21082.
11. Lee, J.; Lee, T. S.; Ryu, J.; Hong, S.; Kang, M.; Im, K.; Kang, J. H.; Lim, S. M.; Park, S.; Song, R. RGD Peptide–Conjugated Multimodal $NaGdF_4$:Yb^{3+}/Er^{3+} Nanophosphors for Upconversion Luminescence, MR, and PET Imaging of Tumor Angiogenesis. *J. Nucl. Med.* **2013**, *54*, 96–103.
12. Liu, C. Y.; Gao, Z. Y.; Zeng, J. F.; Hou, Y.; Fang, F.; Li, Y. L.; Qiao, R. R.; Shen, L.; Lei, H.; Yang, W. S.; Gao, M. Y. Magnetic/Upconversion Fluorescent $NaGdF_4$:Yb,Er Nanoparticle-Based Dual-Modal Molecular Probes for Imaging Tiny Tumors *in Vivo*. *ACS nano* **2013**, *7*, 7227–7240.
13. Chen, H. Y.; Qi, B.; Moore, T.; Colvin, D. C.; Crawford, T.; Gore, J. C.; Alexis, F.; Mefford, O. T.; Anker, J. N. Synthesis of Brightly PEGylated Luminescent Magnetic Upconversion Nanophosphors for Deep Tissue and Dual MRI Imaging. *Small* **2014**, *10*, 160–168.
14. Zeng, S. J.; Xiao, J. J.; Yang, Q. B.; Hao, J. H. Bi-Functional $NaLuF_4$:Gd^{3+}/Yb^{3+}/Tm^{3+} Nanocrystals: Structure Controlled Synthesis, Near-Infrared Upconversion Emission and Tunable Magnetic Properties. *J. Mater. Chem.* **2012**, *22*, 9870–9874.
15. Zhou, J.; Zhu, X.; Chen, M.; Sun, Y.; Li, F. Y. Water-Stable $NaLuF_4$-Based Upconversion Nanophosphors with Long-Term Validity for Multimodal Lymphatic Imaging. *Biomaterials* **2012**, *33*, 6201–6210.
16. Wang, H. B.; Lu, W.; Zeng, T. M.; Yi, Z. G.; Rao, L.; Liu, H. R.; Zeng, S. J. Multi-Functional $NaErF_4$:Yb Nanorods: Enhanced Red Upconversion Emission, *in Vitro* Cell, *in Vivo* X-Ray, and T_2-Weighted Magnetic Resonance Imaging. *Nanoscale*, **2014**, *6*, 2855–2860.
17. Das, G. K.; Zhang, Y.; D'Silva, L.; Padmanabhan, P.; Heng, B. C.; Loo, J. S. C.; Selvan, S. T.; Bhakoo, K. K.; Tan, T. T. Y. Single-Phase Dy_2O_3:Tb^{3+} Nanocrystals as Dual-Modal Contrast Agent for High Field Magnetic Resonance and Optical Imaging. *Chem. Mater.* **2011**, *23*, 2439–2446.
18. Xue, Z.; Yi, Z.; Li, X.; Li, Y.; Jiang, M.; Liu, H. Upconversion Optical/Magnetic Resonance Imaging-Guided Small Tumor Detection and in Vivo Tri-Modal Bioimaging based on High-Performance Luminescent Nanorods. *Biomaterials* **2017**, *115*, 90–103.

19. Li, X.; Yi, Z.; Xue, Z.; Zeng, S.; Liu, H. Multifunctional $BaYbF_5$: Gd/Er Upconversion Nanoparticles for *in Vivo* Tri-Modal Upconversion Optical, X-Ray Computed Tomography and Magnetic Resonance Imaging. *Mater. Sci. Eng. C* **2017**, *75*, 510–516.
20. Feng, Y.; Chen, H.; Ma, L.; Shao, B.; Zhao, S.; Wang, Z. Surfactant-Free Aqueous Synthesis of Novel Ba_2GdF_7:Yb^{3+}, Er^{3+}@PEG Upconversion Nanoparticles for in Vivo Trimodality Imaging. *ACS Appl. Mater. Interfaces* **2017**, *9*, 1–17.
21. Liu, Q.; Sun, Y.; Li, C. G.; Zhou, J.; Li, C. Y.; Yang, T. S.; Zhang, X. Z.; Yi, T.; Wu, D. M.; Li, F. Y. ^{18}F-Labeled Magnetic-Upconversion Nanophosphors via Rare-Earth Cation-Assisted Ligand Assembly. *ACS Nano* **2011**, *5*, 3146–3157.
22. Meenambal, R.; Kannan, S. Cosubstitution of Lanthanides (Gd^{3+}/Dy^{3+}/Yb^{3+}) in β-$Ca_3(PO_4)_2$ for Upconversion Luminescence, CT/MRI Multimodal Imaging. *ACS Biomater. Sci. Eng.* **2017**, 47–56.
23. Deng, H. L.; Huang, S.; Xu, C. Intensely Red-Emitting Luminescent Upconversion Nanoparticles for Deep-Tissue Multimodal Bioimaging. *Talanta*, **2018**, 1–22.

Table S3. Applications of Gd-MOFs and Tm-MOFs.

Metal ions	Ligand	Structure	Application	Ref
Gd^{3+}	N-(4-carboxybenzyl)-(3,5-dicarboxyl)pyridinium bromide ($H_3CmdcpBr$)	$\{[Gd(Cmdcp)-(H_2O)_3](NO_3)\cdot 3H_2O\}_n$	In vivo MRI	1
	1,4-benzenedicarboxylate and 1,2,4-benzenetricarboxylate methyl ammonium salts	Gd MOF	MRI	2
	PT1	$[Gd_6(\mathbf{PT1})_4(NO_3)_6\text{-}9H]^{3+}$	MRI glucosamine	3
	1,4-bis(5-carboxy-1H-benzimidazole-2yl)benzene (pDBI)	Gd-pDBI	Bimodal MRI	4
	1,4-BDC	Gd•(1,4-BDC)	Targeting and MRI	5
	terephthalic acid	Gd-MOF	Bimodal MRI	6
	Benzenehexacarboxylatemoiety (bhc)	$[Gd_2(bhc)(H_2O)_8](H_2O)_2$	Multimodal imaging	7
Tm^{3+}	5-(4-carboxy-2-nitrophenoxy)-isophthalic acid (H_3L)	$[TmL(DMF)_2]\cdot 0.25H_2O$	—	8
	1,3,5-tris(4-carboxyphenyl)-2,4,6-trimethylbenzene (H_3L)	$[Tm_2(L)_2(H_2O)_3]\cdot 2H_2O$	Sensing and adsorption	9
	1,3,5-benzenetricarboxylic acid	$Tm(BTC)(DMF)_2\cdot H_2O$	—	10
	1,4-benzenedicarboxylic acid (H_2BDC)	$Tm_2(TBDC)_3(DMF)_2(H_2O)_2\cdot 4H_2O$	Adsorption	11

	1,10-phenanthroline, 2,2′-bipyridine, or triphenyl phosphate oxide	$Ln(tta)_3L$	—	12
	succinic acid (H_2L)	$[Tm_2(L)_3(H_2O)_2]\bullet H_2O$	—	13
	monophenanthroline	Tm(acetylacetonato)$_3$ monophenanthroline	—	14
	tris-(dibenzoylmethanato)-mono-(bathophenanthroline)	Tm(DBM)$_3$bath	—	15
Gd^{3+}, Tm^{3+}	1,3,5-benzenetricarboxylic acid	$(Gd^{3+},Tm^{3+})(BTC)\bullet(H_2O)\bullet DMF$	drug delivery, UCL and MRI	**This work**

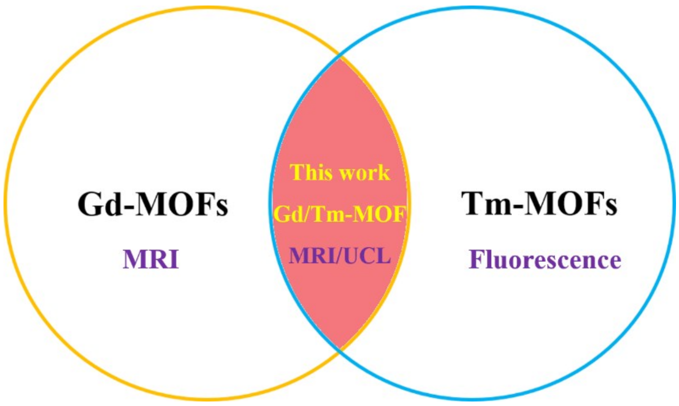

Figure S3. Pie chart of reports on application of Gd-MOFs and Tm-MOFs.

References:

1. Qin, L.; Sun, Z. Y.; Cheng, K.; Liu, S. W.; Pang, J. X.; Xia, L. M.; Chen, W. H.; Cheng, Z.; Chen, J.X. Zwitterionic Manganese and Gadolinium Metal-Organic Frameworks as Efficient Contrast Agents for *in Vivo* Magnetic Resonance Imaging. *ACS Appl. Mater. Interfaces* **2017**, *9*, 1–9.
2. Hatakeyama, W.; Sanchez, T. J.; Rowe, M. D.; Serkova, N. J.; Liberatore, M. W.; Boyes, S. G. Synthesis of Gadolinium Nanoscale Metal-Organic Framework with Hydrotropes: Manipulation of Particle Size and Magnetic Resonance Imaging Capability. *ACS Appl. Mater. Interfaces* **2011**, *3*, 1502–1510.
3. He, C.; Wu, X.; Kong, J. C.; Liu, T.; Zhang, X. L.; Duan, C. Y. A Hexanuclear Gadolinium-Organic Octahedron as a Sensitive MRI Contrast Agent for Selectively Imaging Glucosamine in Aqueous Media. *Chem. Commun.* **2012**, *48*, 9290–9292.
4. Kundu, T.; Mitra, S.; Díaz Díaz, D.; Banerjee, R. Gadolinium(III)-Based Porous Luminescent

Metal–Organic Frameworks for Bimodal Imaging. *ChemPlusChem,* **2016**, *81*, 728–732.

5. Rowe, M. D.; Thamm, D. H.; Kraft, S. L.; Boyes, S. G. Polymer-Modified Gadolinium Metal-Organic Framework Nanoparticles Used as Multifunctional Nanomedicines for the Targeted Imaging and Treatment of Cancer. *Biomacromolecules* **2009**, *10*, 983–993.
6. Tian, C. X.; Zhu, L. P.; Feng, L.; Boyes, S. G. Poly(acrylic acid) Bridged Gadolinium Metal-Organic Framework-Gold Nanoparticle Composites as Contrast Agents for Computed Tomography and Magnetic Resonance Bimodal Imaging. *ACS Appl. Mater. Interfaces* **2015**, *7*, 17765.
7. Taylor, K. M.; Jin, A.; Lin, W. Surfactant-Assisted Synthesis of Nanoscale Gadolinium Metal-Organic Frameworks for Potential Multimodal Imaging. *Angew. Chem. Int. Ed.* **2008**, *47*, 7722–7725.
8. Su, S. Q.; Wang, S.; Song, X. Z.; Song, S. Y.; Qin, C.; Zhu, M.; Hao, Z. M.; Zhao, S. N.; Zhang, H. J. Syntheses, Structures, Photoluminescence, and Magnetic Properties of (3,6)- and 4-Connected Lanthanide Metal-Organic Frameworks with a Semirigid Tricarboxylate Ligand. *Dalton Trans.* **2012**, *41*, 4772–4779.
9. Wang, X. Q.; Zhang, L. L.; Yang, J., Liu, F. L.; Dai, F. N.; Wang, R. M.; Sun, D. F. Lanthanide Metal–Organic Frameworks Containing a Novel Flexible Ligand for Luminescence Sensing of Small Organic Molecules and Selective Adsorption. *J. Mater. Chem. A* **2015**, *3*, 12777–12785.
10. Li, Z. Y.; Zhu, G. S.; Guo, X. D.; Zhao, X. J.; Jin, Z.; Qiu, S. L. Synthesis, Structure, and Luminescent and Magnetic Properties of Novel Lanthanide Metal-Organic Frameworks with Zeolite-like Topology. *Inorg. Chem.* **2007**, *46*, 5174–5178.
11. He, H.; Yuan, D.; Ma, H.; Sun, D.; Zhang, G.; Zhou, H. C. Control over Interpenetration in Lanthanide−Organic Frameworks: Synthetic Strategy and Gas-Adsorption Properties. *Inorg. Chem.* **2010**, *49*, 7605–7607.
12. Dang, S.; Sun, L.N.; Zhang, H.J.; Guo, X.M.; Li, Z.F.; Feng, J.; Guo, H.D.; Guo, Z.Y. Near-Infrared Luminescence from Sol−Gel Materials Doped with Holmium(III) and Thulium(III) Complexes. *J. Phys. Chem. C* **2008**, *112*, 13240–13247.
13. Oliveira, C. A. F. D.; Silva, F. F. D.; Malvestiti, I.; Malta, V. R. D. S.; Dutra, J. D. L.; Jr, N. B. D. C.; Freire, R. O.; Júnior, S. A. Effect of Temperature on Formation of Two New Lanthanide Metal-Organic Frameworks: Synthesis, Characterization and Theoretical Studies of Tm(III)-Succinate. *J. Solid State Chem.* **2013**, *197*, 7–13.
14. Hong, Z. R.; Li, W. L.; Zhao, D. X.; Liang, C. J.; Liu, X. Y.; Peng, J. B.; Zhao, D. Spectrally-Narrow Blue Light-Emitting Organic Electroluminescent Devices Utilizing Thulium Complexes. *Synthetic Metals,* **1999**, *104*, 165–168.
15. Zang, F. X.; Hong, Z. R.; Li, W. L.; Li, M. T.; Sun, X. Y. 1.4 μm Band Electroluminescence from Organic Light-Emitting Diodes Based on Thulium Complexes. *Appl. Phys. Lett.* **2004**, *84*, 2679–2681.

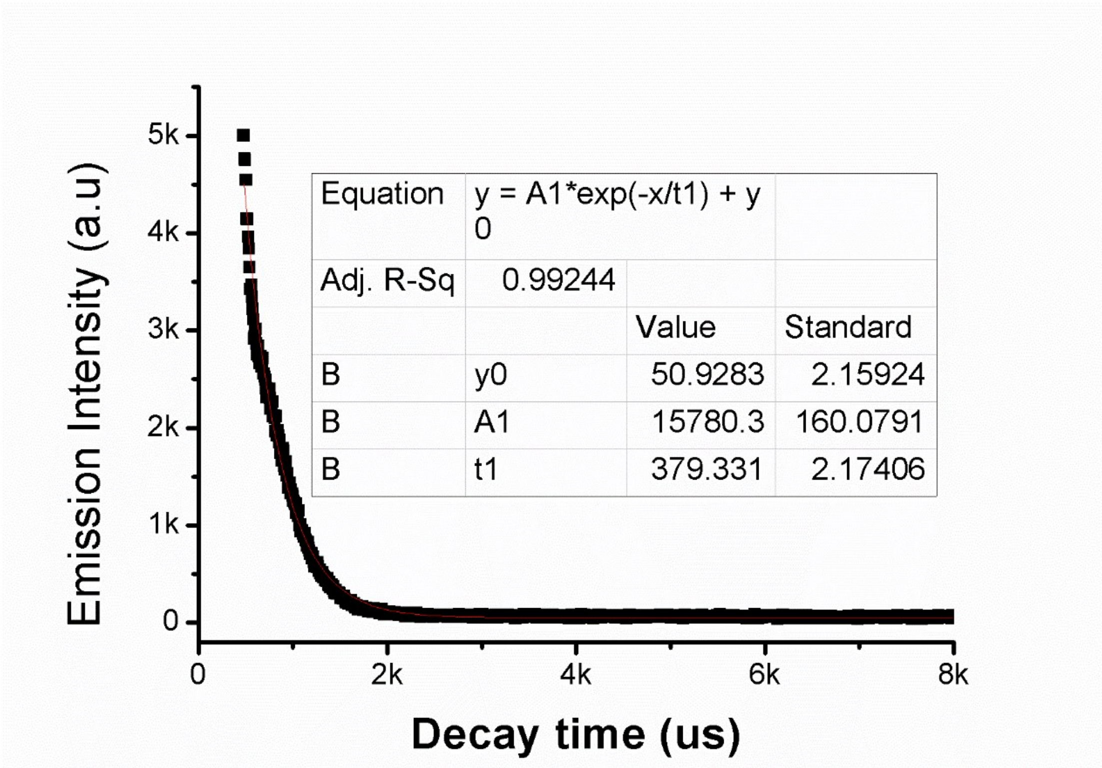

Figure S4. The decay curves for the $^1D_2 \rightarrow ^3F_4$ emissions of Tm^{3+} in Gd/Tm-MOFs.

Table S4. Selected bond lengths [Å] and angles [°] for RE(BTC)•(H_2O)•DMF.

RE(1)-O(3)#1	2.317(3)
RE(1)-O(3)#2	2.317(3)
RE(1)-O(1)	2.323(4)
RE(1)-O(1)#3	2.323(4)
RE(1)-O(2)#4	2.335(4)
RE(1)-O(2)#5	2.335(4)
RE(1)-O(4)	2.438(6)
O(2)-RE(1)#6	2.335(4)
O(3)-RE(1)#7	2.318(3)
O(3)#1-RE(1)-O(3)#2	138.74(19)
O(3)#1-RE(1)-O(1)	146.05(13)
O(3)#2-RE(1)-O(1)	74.92(13)
O(3)#1-RE(1)-O(1)#3	74.92(13)
O(3)#2-RE(1)-O(1)#3	146.05(13)
O(1)-RE(1)-O(1)#3	72.20(18)
O(3)#1-RE(1)-O(2)#4	90.07(15)
O(3)#2-RE(1)-O(2)#4	84.15(14)
O(1)-RE(1)-O(2)#4	89.66(16)
O(1)#3-RE(1)-O(2)#4	103.70(15)
O(3)#1-RE(1)-O(2)#5	84.15(14)
O(3)#2-RE(1)-O(2)#5	90.07(15)
O(1)-RE(1)-O(2)#5	103.70(15)
O(1)#3-RE(1)-O(2)#5	89.66(16)
O(2)#4-RE(1)-O(2)#5	163.6(2)
O(3)#1-RE(1)-O(4)	69.37(10)
O(3)#2-RE(1)-O(4)	69.37(10)
O(1)-RE(1)-O(4)	143.90(9)

O(1)#3-RE(1)-O(4)	143.90(9)
O(2)#4-RE(1)-O(4)	81.79(11)
O(2)#5-RE(1)-O(4)	81.79(11)
C(5)-O(1)-RE(1)	175.0(3)
C(5)-O(2)-RE(1)#6	123.4(3)
C(6)-O(3)-RE(1)#7	149.2(3)
RE(1)-O(4)-H(4A)	109.3

Symmetry transformations used to generate equivalent atoms:

#1 x,y-1,z #2 y,x-1,-z+5/4 #3 y+1,x-1,-z+5/4 #4 -y+1,x-1,z-1/4 #5 x,-y,-z+3/2

#6 y+1,-x+1,z+1/4 #7 x,y+1,z

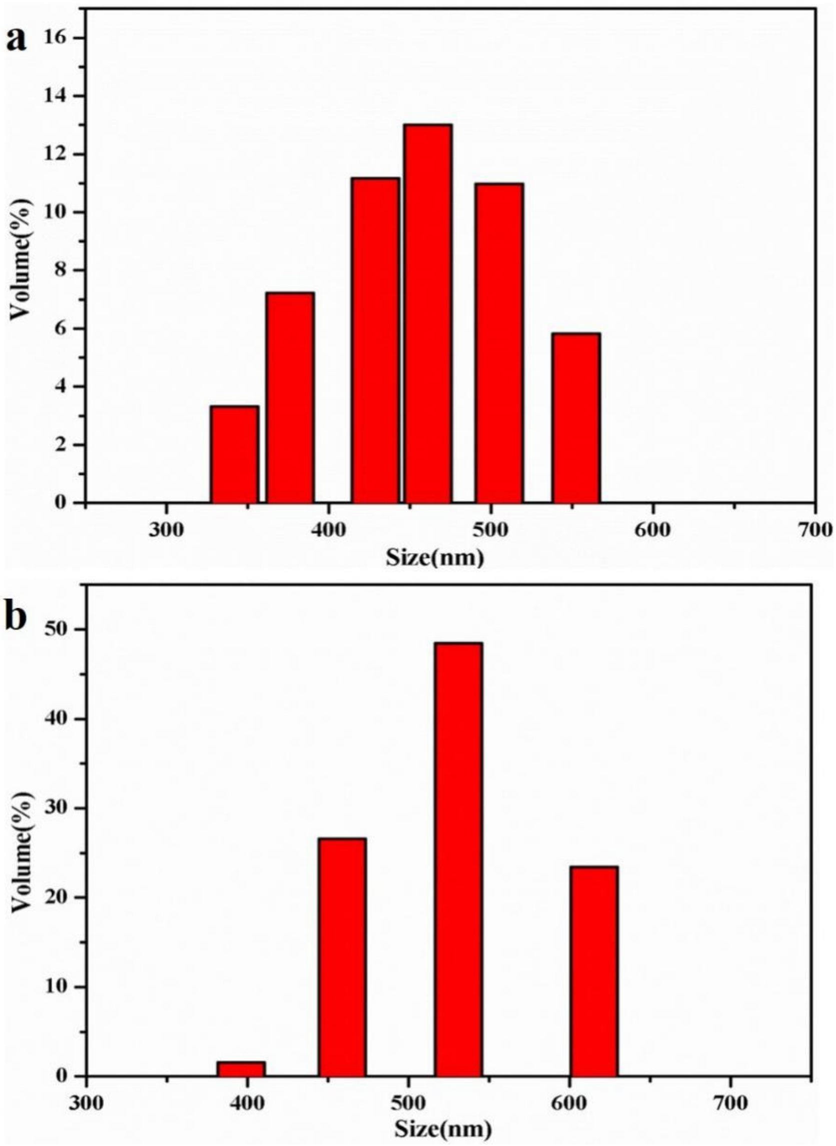

Figure S5. The dynamic light scattering (DLS) of Gd/Tm-MOFs, Gd/Tm-MOFs@mSiO_2, respectively. The DLS suggests that the average width of Gd/Tm-MOFs was 450 nm and the width of Gd/Tm-MOFs@mSiO_2 was around 530 nm approximately. It demonstrates that the thickness of mesoporous SiO_2 shell was about 40 nm.

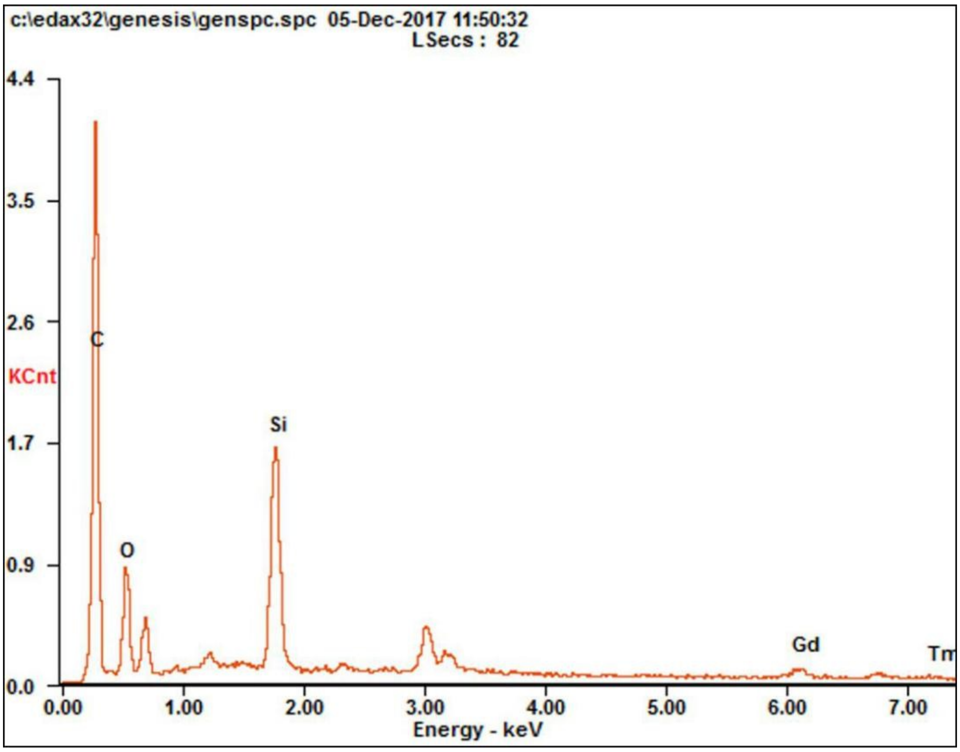

Figure S6. The EDS of Gd/Tm-MOFs@mSiO_2-FA. It determines that the elements of C, O, Si, Gd and Tm are distributed in Gd/Tm-MOFs@mSiO_2-FA composites.

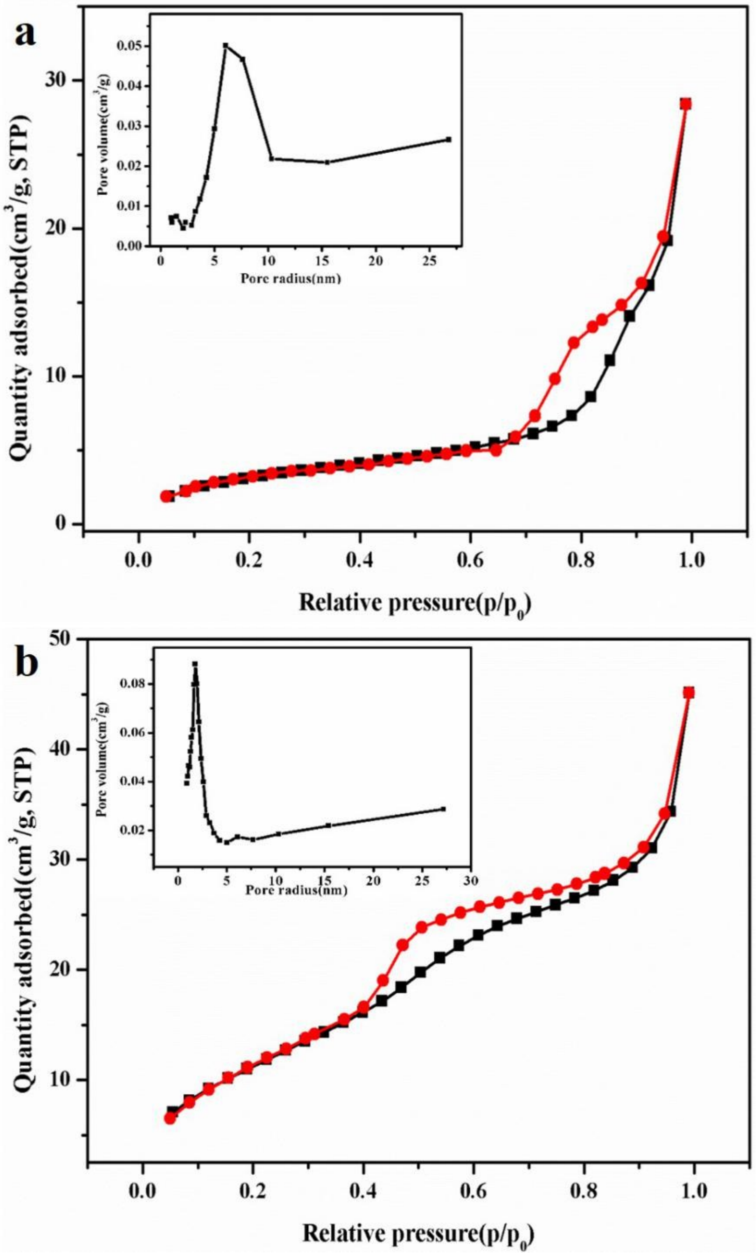

Figure S7. N_2 adsorption (black symbols) and desorption (red symbols) isotherm (a, b) of Gd/Tm-MOFs measured at 77 K and the inset was BJH pore-size distributions of Gd/Tm-MOFs, Gd/Tm-MOFs@mSiO_2, respectively. The surface area of Gd/Tm-MOFs and Gd/Tm-MOFs@mSiO_2-FA is 22.48 m^2/g and 43.71 m^2/g respectively.

Table S5. List of composites based on the mesoporous silica for DOX delivery.

Materials	DOX release percent (%)		The difference (%)	Ref
	Simulation pH of normal cells	Simulation pH of cancer cells		
Fe_3O_4@GO@mSiO_2	96	100	4	1
MSN-PEG	37	45	8	2
ICG/MSN@p(NIPAM-*co*-MA)	33	44.9	11.9	3
MSN	5	20	15	4
Pd@Ag@sSiO_2@mSiO_2	7.2	26	18.8	5
MSN-NH_2	45	69	24	6
MSN@PEM	9	34.25	25.25	7
MSN@PDA-PEG	35.5	65.5	30	8
HMSNs	3.5	37.5	34	9
sericin-coated MSNs	16.4	53.9	37.5	10
MSN@Gelatin	4	44	40	11
GQD-MSNs	7.4	48.6	41.2	12
PB@mSiO_2-PEG	3.1	46.6	43.5	13
α-CD@PEG-*g*-chitosan/Fe_3O_4@GO@SiO_2	45	98	43	14
Ag-MSNs	5	50	45	15
$MnFe_2O_4$@HMSN@YbL (TTA)@DOX@cCTS	33.4	81.4	48	16
HPSN-Salphdc-FA	10	60	50	17
PDEAEMA-HMSNs	12	64	52	18
MSNs-NH-N=C-HA	10.12	65.62	55.5	19
MSN-PAA	10	70	60	4
MSN-PMA_{SH}	25	88	63	20
PAH/PSS-MSNTs	25	90	65	21
PAH-cit/APTES-MSNs	20	88	68	22

MSN@PSA-PEG-FA	5.8	78.4	72.6	23
CPT@MSN-hyd	15	90	75	24
Gd/Tm-MOF@SiO_2-FA	12	64	52	**This work**

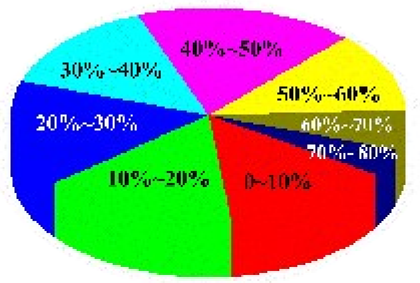

Figure S8. Pie chart of distribution DOX release percent.

References:

1. Pourjavadi, A.; Tehrani, Z. M.; Jokar, S. Functionalized Mesoporous Silica-Coated Magnetic Graphene Oxide by Polyglycerol-g-Polycaprolactone with pH-Responsive Behavior: Designed for Targeted and Controlled Doxorubicin Delivery. *J. Ind. Eng. Chem.* **2015**, *28*, 45–53.
2. Zhang, Q.; Zhao, H. Y.; Li, D.; Liu, L. P.; Du, S. H. A Surface-Grafted Ligand Functionalization Strategy for Coordinate Binding of Doxorubicin at Surface of PEGylated Mesoporous Silica Nanoparticles: Toward pH-Responsive Drug Delivery. *Colloids Surf., B,* **2016**, *149*, 138–145.
3. Shu, Y.; Song, R. S.; Zheng, A. Q.; Huang, J. L.; Chen, M. L.; Wang, J. H. Thermo/pH Dual-Stimuli-Responsive Drug Delivery for Chemo-/Photothermal Therapy Monitored by Cell Imaging. *Talanta,* **2018**, *181*, 278–285.
4. Yuan, L.; Tang, Q. Q.; Yang, D.; Zhang, J. Z.; Zhang, F. Y.; Hu, J. H. Preparation of pH-Responsive Mesoporous Silica Nanoparticles and Their Application in Controlled Drug Delivery. *J. Phys. Chem. C,* **2011**, *115*(20), 9926–9932.
5. Fang, W. J.; Yang, J.; Gong, J. W.; Zheng, N. F. Photo-and pH-Triggered Release of Anticancer Drugs from Mesoporous Silica-Coated Pd@Ag Nanoparticles. *Adv. Funct. Mater.* **2012**, *22*, 842–848.
6. Wu, X.; Wang, Z. Y.; Zhu, D.; Zong, S. F.; Yang, L. P.; Zhong, Y.; Cui, Y. P. pH and Thermo Dual-Stimuli-Responsive Drug Carrier Based on Mesoporous Silica Nanoparticles Encapsulated in a Copolymer–Lipid Bilayer. *ACS Appl. Mater. Interfaces,* **2013**, *5*(21), 10895–10903.
7. Wang, J.; Liu, H. Y.; Leng, F.; Zheng, L. L.; J. Yang, H.; Wang, W.; Huang, C. Z.

Autofluorescent and pH-Responsive Mesoporous Silica for Cancer-Targeted and Controlled Drug Release. *Microporous Mesoporous Mater.* **2014**, *186*, 187–193.

8. Li, X. R.; Garamus, V. M.; Li, N.; Gong, Y. B.; Zhe, Z.; Tian, Z. F.; Zou, A. H. Preparation and Characterization of a pH-Responsive Mesoporous Silica Nanoparticle Dual-Modified with Biopolymers. *Colloids Surf., A,* **2018**.
9. Gao, Y.; Chen, Y.; Ji, X. F.; He, X. Y.; Yin, Q.; Zhang, Z. W.; Shi, J. L.; Li, Y. P. Controlled Intracellular Release of Doxorubicin in Multidrug-Resistant Cancer Cells by Tuning the Shell-Pore Sizes of Mesoporous Silica Nanoparticles. *ACS Nano*, **2011**, *5*, 9788–9798.
10. Liu, J.; Li, Q. L.; Zhang, J. X.; Huang, L.; Qi, C.; Xu, L. M.; Liu, X. X.; Wang, G. B.; Wang, L.; Wang, Z. Safe and Effective Reversal of Cancer Multidrug Resistance Using Sericin-Coated Mesoporous Silica Nanoparticles for Lysosome-Targeting Delivery in Mice. *Small*, **2017**, *13*, 1602567 1–14.
11. Zou, Z.; He, D. G.; He, X. X.; Wang, K. M.; Yang, X.; Zhou, Q. Natural Gelatin Capped Mesoporous Silica Nanoparticles for Intracellular Acid-Triggered Drug Delivery. *Langmuir*, **2013**, *29*, 12804–12810.
12. Yao, X. X.; Tian, Z. F.; Liu, J. X.; Zhu, Y. F.; Hanagata, N. Mesoporous Silica Nanoparticles Capped with Graphene Quantum Dots for Potential Chemo–Photothermal Synergistic Cancer Therapy. *Langmuir*, **2017**, *33*, 591–599.
13. Su, Y. Y.; Teng, Z. G.; Yao, H.; Wang, S. J.; Tian, Y.; Zhang, Y. L.; Liu, W. F.; Tian, W.; Zheng, L. J.; Lu, N.; Ni, Q. Q.; Su, X. D.; Tang, Y. X.; Sun, J.; Liu, Y.; Wu, J.; Yang, G. F.; Lu, G. M.; Zhang, L. J. A Multifunctional PB@mSiO_2–PEG/DOX Nanoplatform for Combined Photothermal–Chemotherapy of Tumor. *ACS Appl. Mater. Interfaces* **2016**, *8*, 17038–17046.
14. Pourjavadi, A.; Tehrani, Z. M.; Jokar, S. Chitosan Based Supramolecular Polypseudorotaxane as a pH-Responsive Polymer and Their Hybridization with Mesoporous Silica-Coated Magnetic Graphene Oxide for Triggered Anticancer Drug Delivery. *Polymer*, **2015**, *76*, 52–61.
15. Shao, D.; Zhang, X.; Liu, W. L.; Zhang, F.; Zheng, X.; Qiao, P.; Li, J.; Dong, W. F.; Chen, L. Janus Silver-Mesoporous Silica Nanocarriers for SERS Traceable and pH-Sensitive Drug Delivery in Cancer Therapy. *ACS Appl. Mater. Interfaces* **2016**, *8*, 4303–4308.
16. Shan, C. F.; Wang, B. K.; Hu, B. B.; Liu, W. S.; Tang, Y. Smart Yolk-Shell Type Luminescent Nanocomposites Based on Rare-Earth Complex for NIR–NIR Monitor of Drug Release in Chemotherapy. *J. Photochem. Photobiol., A,* **2018**, *355*, 233–241.
17. Dai, L. L.; Zhang, Q. F.; Li, J. H.; Shen, X. K.; Mu, C. Y.; Cai, K. Y. Dendrimerlike Mesoporous Silica Nanoparticles as pH-Responsive Nanocontainers for Targeted Drug Delivery and Bioimaging. *ACS Appl. Mater. Interfaces* **2015**, *7*, 7357–7372.
18. Zhang, Y. Y.; Ang, C. Y.; Li, M. H.; Tan, S. Y.; Qu, Q. Y.; Luo, Z.; Zhao, Y. L. Polymer-Coated Hollow Mesoporous Silica Nanoparticles for Triple-Responsive Drug Delivery. *ACS*

Appl. Mater. Interfaces **2015**, *7*, 18179–18187.

19. Chen, C.; Sun, W.; Wang, X. L.; Wang, Y. B.; Wang, P. pH-Responsive Nanoreservoirs Based on Hyaluronic Acid End-Capped Mesoporous Silica Nanoparticles for Targeted Drug Delivery. *Int. J. Biol. Macromol.* **2018**, *111*, 1106–1115.
20. Cui, J. W.; Yan, Y.; Wang, Y. J.; Caruso, F. Templated Assembly of pH-Labile Polymer-Drug Particles for Intracellular Drug Delivery. *Adv. Funct. Mater.* **2012**, *22*, 4718–4723.
21. Yang, Y. J.; Tao, X.; Hou, Q.; Ma, Y.; Chen, X. L.; Chen, J. F. Mesoporous Silica Nanotubes Coated with Multilayered Polyelectrolytes for pH-Controlled Drug Release. *Acta Biomaterialia,* **2010**, *6*, 3092–3100.
22. Zhang, P.; Wu, T.; J. L. Kong, In Situ Monitoring of Intracellular Controlled Drug Release from Mesoporous Silica Nanoparticles Coated with pH-Responsive Charge-Reversal Polymer. *ACS Appl. Mater. Interfaces* **2014**, *6*, 17446–17453.
23. Yang, K.; Luo, H. Q.; Zeng, M.; Jiang, Y. Y.; Li, J. M.; Fu, X. L. Intracellular pH-Triggered, Targeted Drug Delivery to Cancer Cells by Multifunctional Envelope-Type Mesoporous Silica Nanocontainers. *ACS Appl. Mater. Interfaces* **2015**, *7*, 17399–17407.
24. Li, Z. Y.; Liu, Y.; Wang, X. Q.; Liu, L. H.; Hu, J. J.; Luo, G. F.; Chen, W. H.; Rong, L. X.; Zhang, Z. One-Pot Construction of Functional Mesoporous Silica Nanoparticles for the Tumor-Acidity-Activated Synergistic Chemotherapy of Glioblastoma. *ACS Appl. Mater. Interfaces* **2013**, *5*, 7995–8001.

Table S6. List of Gd^{3+} as excellent T_1-MRI contrast agents.

Materials	r_1 value ($mM^{-1}•s^{-1}$)	Ref
β-$NaYF_4$:Yb,Gd,Tm	0.853	1
Gd-PEI	2.1	2
Gd-DOTA	3	3
Gadolinium (Gd)-based bacteria	4.1	4
$NaGdF_4$:Yb/Tm@SiO_2@TiO_2	4.53	5
Gd•(terephthalic acid)	4.55	6
Gd-DTPA (widely used in clinic MRI)	5.77	7
gemcitabine-5’ -monophosphate/Gd^{3+}-PEG	8.3	8
Gd•(1,4-BDC)	9.86	9
PPy@BSA-Gd	10.203	10
Gd-pDBI	12.33	11
$\{[Gd(Cmdcp)\text{-}(H_2O)_3](NO_3)\cdot 3H_2O\}_n$	13.46	12
GRGDS-NH_2+MTX-copolymer-modified Gd MOF nanoparticles	14.45	9
$[DPP\text{-}ZnP\text{-}GdDOTA]^-$	19.94	13
Au core-silica layer/Gd^{3+}-Au shell	24	3
PNIPAM-co-PNAOS-co-PFMA modified Gd-MOF nanoparticles	33.43	9
MTX-copolymer-modified Gd MOF nanoparticles	38.52	9
Gd-AuNCs	41.5±2.5	14
Gd^{3+}/Dy^{3+}/Yb^{3+} cosubstitutions in β-$Ca_3(PO_4)_2$	48.71	15
PEG-Na_xGdWO_3	80	16
Gd•(1,2,4-BTC)	83.9	17
$[Gd_6(\mathbf{PT1})_4(NO_3)_6\text{-}9H]^{3+}$	388.5	18
(Gd, Tm) • (BTC)•(H_2O)•DMF	225.86	**This work**

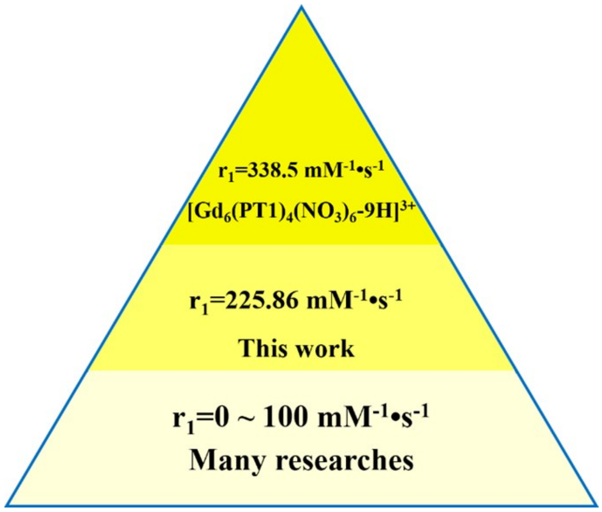

Figure S9. Pie chart of reports on Gd^{3+} as T_1-MRI contrast agents.

References:

2. Wang, X.; Chen, J. T.; Zhu, H.; Chen, X.; Yan, X. P. One-step Solvothermal Synthesis of Targetable Optomagnetic Upconversion Nanoparticles for *in Vivo* Bimodal Imaging. *Anal. Chem.* **2013**, *85*, 10225–10232.
3. Lim, C. K.; Singh, A.; Heo, J.; Kim, D.; Lee, K. E.; Jeon, H.; Koh, J.; Kwon, I. C.; Kim, S. Gadolinium-Coordinated Elastic Nanogels for *in Vivo* Tumor Targeting and Imaging. *Biomaterials* **2013**, *34*, 6846-6852.
4. Marangoni, V. S.; Neumann, O.; Henderson, L.; Kaffes, C. C.; Zhang, H.; Zhang, R. M.; Bishnoi, S.; Zucolotto, V.; Bankson, J. A.; Nordlander, P. Enhancing T1 Magnetic Resonance Imaging Contrast with Internalized Gadolinium (III) in a Multilayer Nanoparticle. *Proc. Nat. Acad. Sci.* **2017**, *114*, 6960–6965.
5. Zhang, L. L.; Liu, Y.; Zhang, Q. Y.; Li, T. G.; Yang, M.; Yao, Q. Q.; Hu, H. Y. Gadolinium-Labelled Aminoglycoside and its Potential Application as a Bacteria-Targeting Magnetic Resonance Imaging Contrast Agent. *Anal. Chem.* **2018**, 1–7.
6. Zhang, L. E.; Zeng, L. Y.; Pan Y. W.; Luo, S.; Ren, W. Z.; Gong, A.; Ma, X. H.; Liang, H. Z.; Lu, G. M.; Wu, A. G. Inorganic Photosensitizer Coupled Gd-Based Upconversion Luminescent Nanocomposites for in Vivo Magnetic Resonance Imaging and Near-Infrared-Responsive Photodynamic Therapy in Cancers. *Biomaterials* **2015**, *44*, 82–90.
7. Tian, C. X.; Zhu, L. P.; Feng, L.; Boyes, S. G. Poly(acrylic acid) Bridged Gadolinium Metal-Organic Framework-Gold Nanoparticle Composites as Contrast Agents for Computed Tomography and Magnetic Resonance Bimodal Imaging. *ACS Appl. Mater. Interfaces* **2015**, *7*, 17765.
8. Zhou, J.; Sun, Y.; Du, X. X.; Xiong, L. Q.; Hu, H.; Li, F. Y. Dual-modality *in Vivo* Imaging Using Rare-Earth Nanocrystals with Near-Infrared to Near-Infrared (NIR-to-NIR) Upconversion Luminescence and Magnetic Resonance Properties. *Biomaterials* **2010**, *31*,

3287–3295.

9. Li, L. L.; Tong, R.; Li, M. Y.; Kohane, D. S. Self-Assembled Gemcitabine-Gadolinium Nanoparticles for Magnetic Resonance Imaging and Cancer Therapy. *Acta Biomater.* **2016**, *33*, 34–39.
10. Rowe, M. D.; Thamm, D. H.; Kraft, S. L.; Boyes, S. G. Polymer-Modified Gadolinium Metal-Organic Framework Nanoparticles Used as Multifunctional Nanomedicines for the Targeted Imaging and Treatment of Cancer. *Biomacromolecules* **2009**, *10*, 983-993.
11. Yang, Z.; He, W. S.; Zheng, H. Y.; Wei, J. L.; Liu, P.; Zhu, W.; LiN, L. P.; Zhang, L.; Yi, C. F.; Xu, Z. S.; Ren, J. H. One-Pot Synthesis of Albumin-Gadolinium Stabilized Polypyrrole Nanotheranostic Agent for Magnetic Resonance Imaging Guided Photothermal Therapy. *Biomaterials* **2018**.
12. Meenambal, R.; Kannan, S. Cosubstitution of Lanthanides (Gd^{3+}/Dy^{3+}/Yb^{3+}) in β-$Ca_3(PO_4)_2$ for Upconversion Luminescence, CT/MRI Multimodal Imaging. *ACS Biomater. Sci. Eng.* **2017**, *4*, 47–56.
13. Kundu, T.; Mitra, S.; Díaz Díaz, D.; Banerjee, R. Gadolinium(III)-Based Porous Luminescent Metal–Organic Frameworks for Bimodal Imaging. *ChemPlusChem,* **2016**, *81*, 728-732.
14. Qin, L.; Sun, Z. Y.; Cheng, K.; Liu, S. W.; Pang, J. X.; Xia, L. M.; Chen, W. H.; Cheng, Z.; Chen, J. X. Zwitterionic Manganese and Gadolinium Metal-Organic Frameworks as Efficient Contrast Agents for in Vivo Magnetic Resonance Imaging. *Acs Appl Mater Interfaces,* **2017,** *9*, 1-9.
15. Schmitt J.; Heitz V.; Sour A.; Bolze, F.; Kessler, P.; Flamigni, L.; Ventura, B.; Bonnet, C. S.; Tóth, É. A Theranostic Agent Combining a Two-Photon-Absorbing Photosensitizer for Photodynamic Therapy and a Gadolinium(III) Complex for MRI Detection. *Chem. Eur. J.* **2016**, *22*, 2775–2786.
16. Liang, G. H.; Ye, D. X.; Zhang, X. X.; Dong, F.; Chen, H.; Zhang, S.; Li, J. Q.; Shen, X. R.; Kong, J. L. One-Pot Synthesis of Gd^{3+}-Functionalized Gold Nanoclusters for Dual Model (Fluorescence/Magnetic Resonance) Imaging. *J. Mater. Chem. B* **2013**, *1*, 3545–3552.
17. Ni, D. L.; Zhang, J. W.; Wang, J.; Hu, P.; Jin, Y.; Tang, Z. M.; Yao, Z. W.; Bu, W. B.; Shi, J. L. Oxygen Vacancy Enables Markedly Enhanced Magnetic Resonance Imaging-Guided Photothermal Therapy of a Gd^{3+}-Doped Contrast Agent. *ACS Nano* **2017**, *11*, 4256-4264.
18. Hatakeyama, W.; Sanchez, T. J.; Rowe, M. D.; Serkova, N. J.; Liberatore, M. W.; Boyes, S. G. Synthesis of Gadolinium Nanoscale Metal-Organic Framework with Hydrotropes: Manipulation of Particle Size and Magnetic Resonance Imaging Capability. *Acs Appl. Mater. Interfaces* **2011**, *3*, 1502-1510.
19. He, C.; Wu, X.; Kong, J. C.; Liu, T.; Zhang, X. L.; Duan, C. Y. A Hexanuclear Gadolinium-Organic Octahedron as a Sensitive MRI Contrast Agent for Selectively Imaging Glucosamine in Aqueous Media. *Chem. Commun.* **2012**, *48*, 9290-9292.